Journal of Thermal Biology 86 (2019) 102431

Contents lists available at ScienceDirect

Journal of Thermal Biology

journal homepage: http://www.elsevier.com/locate/jtherbio

Numerical study of the effect of vascular bed on heat transfer during high intensity focused ultrasound (HIFU) ablation of the liver tumor

M. Mohammadpour, B. Firoozabadi *

Center of Excellence in Energy Conversion, School of Mechanical Engineering, Sharif University of Technology, Tehran, Iran

ARTICLE INFO

Keywords:
HIFU
Vascular bed
Acoustics-thermal-fluid
Heat transfer
Liver tumor
Vascular density

ABSTRACT

In this study, the influence of vascular bed comprising terminal arterial branches on heat transfer in a liver tumor exposed to high intensity focused ultrasound (HIFU) is studied numerically. Also, the effect of vascular density on temperature distribution is investigated. A coupled set of acoustics, thermal, and fluid models is used to calculate the temperature distribution in the liver. The numerical model is established based on the Westervelt and bioheat equations along with the Navier-Stokes equations. Moreover, the acoustic streaming effect is included with Newtonian and non-Newtonian flow assumptions. It is found that in a vascular bed comprising terminal arterial branches, the effect of acoustic streaming is negligible because of the small diameter of these vessels, and the non-Newtonian behavior of blood flow reduces the peak streaming velocity. It is also shown that the vascular density (amount of tissue vascular content) has a considerable cooling effect on peak temperature and hence lesion volume in the liver and, by increasing the vascular density, the treatment duration is prolonged. Results show that when the tumor is embedded in the vascular bed, the cancer cells near the vessels walls remain viable. Some approaches are proposed and compared to improve the efficacy of HIFU in a tumor located in the vascular bed. These approaches include increasing the source pressure or transducer gain. It is concluded that for the assumed configuration of the vascular bed, adjusting the transducer gain is preferred to increase the lesion size and to prevent the problems related to skin burns simultaneously.

1. Introduction

Nowadays, high intensity focused ultrasound (HIFU) is considered a promising approach for non-invasive thermal ablation of tumors. In fact, by optimizing HIFU operation mode, it is possible to concentrate a large amount of acoustic energy in a small volume of tissue and elevate focal zone temperature rapidly. In this manner, the surrounding healthy tissues remain unaffected or indicate a negligible temperature rise (Al-Bataineh et al., 2012; Bailey et al., 2003; Curra et al., 2000; Solovchuk et al., 2013a). In recent years, HIFU has been employed to treat different solid tumors such as liver, pancreas, breast, prostate, and brain in clinics. The primary mechanism of HIFU ablation is thermal coagulation due to absorption of ultrasound wave during propagation and conversion to heat. The temperature in the focal zone should be between 60 $^{\circ}C$ (or 55 $^{\circ}C$) and 95 $^{\circ}C$ for thermal coagulation and necrosis to occur (Al-Bataineh et al., 2012; Huang et al., 2015; Solovchuk et al., 2013a; Zhou et al., 2011).

In recent years, the incidence rate of liver cancer has increased sharply for both men and women. Nowadays, liver cancer is the second leading cause of cancer death in the world (Ryerson et al., 2016). Surgical resection is the preferred choice for treatment of malignant hepatic tumors. However, in some cases, the patient is not a suitable candidate for surgical resection because of some reasons, such as the tumor size, multifocal disease, and location of the tumor to key vessels. In these cases, other minimally invasive ablation methods such as radio-frequency ablation, microwave ablation, and HIFU can be used to treat hepatic tumors (Rattanadecho and Keangin, 2013; Sheu et al., 2011; Tungjitkusolmun et al., 2002). In this study, HIFU is only considered because of the lower side effects and more success in ablating the cancerous cells (Sheu et al., 2011). Since the liver is an organ with high blood perfusion, the blood vessels act as heat sinks and the relationship between the heating power applied in the tissue and the focal zone temperature is complex (Chent et al., 1993; Peng et al., 2011). Therefore, it is necessary to assess the liver vessels cooling effect on the outcome of high intensity focused ultrasound ablation.

In most cases, the temperature elevation in a tissue which is under thermal ablation process is modeled by using Pennes bioheat transfer equation (Guntur and Choi, 2015; Irastorza et al., 2017; Mahoney et al.,

* Corresponding author. School of Mechanical engineering, Sharif University of Technology, Azadi Avenue, Tehran, Iran.
E-mail address: firoozabadi@sharif.ir (B. Firoozabadi).

https://doi.org/10.1016/j.jtherbio.2019.102431
Received 4 January 2019; Received in revised form 30 August 2019; Accepted 4 October 2019
Available online 7 October 2019

2001; Meaney et al., 1999; Samanipour et al., 2013; Zhou et al., 2011; Zhou, 2013). In this equation, the cooling effect is estimated based on the perfusion rate in capillaries (Pennes, 1948). The Pennes bioheat equation assumes that blood enters the capillary bed at the temperature of supply vessels and thermally equilibrates with the surrounding tissue. This simplified equation is valid for a tissue comprising microvasculature; However, for a tissue which contains thermally significant vessel (with a diameter larger than 0.5 mm), the homogenization assumption cannot be applied, and the convective cooling effect of the vessels should be considered separately (Curra et al., 2000; Kolios et al., 1996; Sheu et al., 2011; Solovchuk et al., 2013a). Kolios et al. (1996) investigated lesion formation in a tissue exposed to focused ultrasound and the blood flow effect on temperature distribution and lesion dimension. Besides, the effects of both microvasculature and thermally significant vessels were taken into account. Curra et al. (2000) studied the blood flow effect on heat generation and temperature field due to HIFU in a perfused liver tissue. They considered the importance of nonlinear effects on ultrasound propagation and heat generation in the presence of the blood vessel. Based on the results, it was shown that convection heat transfer of blood vessel shifts the highest temperature region in the direction of blood flow. Hariharan et al. (2007) investigated the effect of a large blood vessel on the efficacy of HIFU treatment at moderate intensities by using a 3D computational model. It was demonstrated that lesion volume would be reduced considerably when the blood vessel is within a beam width of the ultrasound beam.

Attenuation of ultrasound waves in a fluid causes a pressure gradient, which results in an additional fluid flow called acoustic streaming. In recent years, acoustic streaming has become important in different biomedical applications, including HIFU therapy. Acoustic streaming is a mechanical effect of HIFU, which alters the profile of the blood flow velocity, and hence, changes the convective cooling of the blood vessel (Huang, 2002). Therefore, in recent years, some studies have been conducted on the effect of acoustic streaming on HIFU therapy.

Huang et al. (2004) considered the effect of blood flow and acoustic streaming on temperature profile in hemostasis application numerically and experimentally. They simulated the acoustic propagation in the tissue using a 2D nonlinear wave equation. However, the temperature and velocity field calculations were conducted based on a 3D model. A 3D acoustics-thermal-fluid coupling model was used by Sheu et al. (2011) and Solovchuk et al. (2012; 2013a; 2013b) to predict the tumor temperature in liver tissue exposed to HIFU. In the study of Sheu et al. (2011), ultrasound propagation was modeled based on the linear Westervelt equation in the patient-specific liver geometry. Also, hemodynamic equations along with terms associated with acoustic streaming phenomenon were solved to obtain the velocity profile of the blood flow. The results showed that acoustic streaming would alter the blood flow profile in arterial branches of the liver. In the study of Solovchuk et al. (2012), a three-dimensional model was used to study the effect of blood flow and acoustic streaming on the temperature field due to HIFU. This model was based on the Westervelt equation, bioheat equation, and nonlinear Navier-Stokes equation. The results showed that the convective cooling and acoustic streaming in the large blood vessels can change the temperature distribution and lesion shape considerably. In another study by Solovchuk et al. (2013a), the effect of different focal point locations and blood vessel diameters was considered on temperature field in the liver tumor during HIFU ablation. It was demonstrated that both convective cooling and acoustic streaming have a considerable impact on the lesion size near large blood vessels, and this effect reduces for smaller diameter ones. Moreover, in another study of Solovchuk et al. (2013b) ultrasound propagation was modeled by using nonlinear Westervelt equation and the blood flow and acoustic streaming effects were investigated on the HIFU therapy of liver tumors. The results demonstrated that acoustic streaming has a considerable impact on the wall temperature of the vein with a diameter of 3 mm. Solovchuk et al. (2014) conducted another study to predict the temperature field in a liver tumor near a 7 mm diameter blood vessel. Based on their results, it was demonstrated that streaming velocity may be much larger than the blood flow velocity in the large diameter blood vessel considered in their study.

In a perfused tissue such as the liver, the tumor may be located in a vascular bed, including different generations of the vessels. In the most previous studies (Hariharan et al., 2007; Sheu et al., 2011; Solovchuk et al., 2012, 2013a, 2013b), the effect of a single large vessel (such as large arteries or large veins) was separately considered on lesion formation during HIFU therapy. However, in these researches, the cooling effect of other generations of the vasculature comprising both micro vessels (such as hepatic arterioles, portal and hepatic venules and capillaries) and macro vessels (such as arterial branches, terminal arterial branches, terminal veins and venous branches) in the vicinity of the tumor was modeled collectively by using simplified Pennes Bioheat transfer model. This simplification (modeling the macro vessels cooling effect by using Pennes equation) reduces the accuracy of HIFU treatment planning. Hence, it is necessary to investigate the effect of different generations of the liver vasculature on the HIFU therapy outcome. To the best of our knowledge, numerical results which consider the impact of the vascular bed, including different generations, on temperature elevation during HIFU ablation have not yet been reported. Therefore, in the present study, as the first step toward this consideration, the cooling effect of a vascular bed of simple geometry comprising terminal arterial branches is investigated. Also, the impact of vascular density (the volume fraction of the vascular space) on temperature distribution and lesion formation is included. It should be noted that this parameter study cannot be done by using Pennes model and therefore, this is a new parameter study to consider the effect of the accumulation of vessels around the tumor on the HIFU efficacy.

Since, acoustic streaming has a significant influence on the cooling effect of blood vessels, the acoustic streaming phenomenon is also considered in the vascular bed. In addition, because blood vessels with a diameter smaller than 1 mm are investigated; the effect of the non-Newtonian behavior of blood flow on the acoustic streaming profile is calculated as well. Finally, some solutions are proposed and compared to improve HIFU efficacy in the treatment of a tumor located in the vascular bed and to have the least amount of cancerous cells remain viable near the blood vessel walls. Although this comparison is conducted based on an idealized geometry, it is a new insight into the improvement of HIFU efficacy in liver tumor ablation and can be matured by analyzing more complex geometries.

2. Materials and methods

2.1. Ultrasound propagation model

In the present study, the linear Westervelt wave equation is utilized to model ultrasound propagation from the transducer to the focal region. The general nonlinear Westervelt equation for the acoustic pressure field (p_a) in a thermo-viscous fluid is given below (Hamilton and Blackstock, 1998):

$$\nabla^2 p_a - \frac{1}{c^2}\frac{\partial^2 p_a}{\partial t^2} + \frac{\delta}{c^4}\frac{\partial^3 p_a}{\partial t^3} + \frac{\beta}{\rho c^4}\frac{\partial^2 p_a^2}{\partial t^2} = 0 \quad (1)$$

In this equation, c, t, δ and β are the speed of sound, time, acoustic diffusivity, coefficient of nonlinearity, respectively. The acoustic diffusivity, δ, is related to the loss due to the viscosity and thermal conductivity of the propagating medium. For a thermo-viscous fluid, acoustic diffusivity can be represented by equation (2) in terms of acoustic absorption coefficient (α). In this equation, ω is the angular frequency of the transducer (Hamilton and Blackstock, 1998). According to equation (2), the absorption coefficient is proportional to the frequency squared. In a thermo-viscous fluid, the ultrasound absorption is due to the thermal and viscous losses. However, it is theorized that the principle

mechanism of ultrasonic absorption in biological tissues is the relaxation process. Therefore, the absorption coefficient of biological tissues has a linear dependence on frequency due to relaxation effects (Shung, 2006). In this study, the relaxation phenomenon is neglected to simplify the acoustic calculations.

$$\delta = \frac{2c^3\alpha}{\omega^2} \tag{2}$$

Also, the coefficient of nonlinearity, β, is related to the acoustic nonlinearity phenomenon which becomes significant at large amplitudes of the ultrasound wave. In the present work, HIFU at a moderate intensity is utilized, and hence, the effect of nonlinearity is neglected for simplifying the acoustic calculations. In this regime, the time-averaged focal intensity is between 100 W/cm^2 and 1000 W/cm^2 and the focal peak negative pressure is in the range of 1 MPa–4 MPa. Also, the nonlinearity parameter (N) which is defined according to (3) is on the order of a few tenths (Hariharan et al., 2007). It should be noted that this parameter (N) is the ratio of the focal length to the plane wave shock formation distance (Curra et al., 2000). In equation (3), d is the focal length, and p_0 is the transducer pressure. Transducer pressure can be calculated based on (4) in terms of the average transducer power ($P_{transducer}$) and is assigned to the transducer surface. In equation (4), $A_{transducer}$ is the transducer surface area. In the present work, the value of the transducer power is chosen to meet the conditions described above and to be at the moderate intensity regime.

$$N = \frac{d\beta\omega p_0}{\rho c^3} \tag{3}$$

$$p_0 = \sqrt{\frac{2\rho c P_{transducer}}{A_{transducer}}} \tag{4}$$

Then, the linear Westervelt equation is solved, and the acoustic pressure field in the whole domain is determined. Also, the acoustic intensity field (I) is calculated based on equation (5). Finally, the heat generation per unit volume (Q) due to HIFU exposure can be calculated by equation (6) (Solovchuk et al., 2013a).

$$I = \frac{p_a^2}{2\rho c} \tag{5}$$

$$Q = 2\alpha I \tag{6}$$

2.2. Hemodynamics model

The blood flow velocity can be obtained by solving hemodynamic equations in blood vessels. Since HIFU can induce an additional flow called acoustic streaming, this effect is also taken into account. Hence, the blood velocity for an incompressible and laminar flow can be obtained based on the equations (7) and (8).

$$\nabla \cdot \vec{u} = 0 \tag{7}$$

$$\frac{\partial \vec{u}}{\partial t} + (\vec{u}\cdot\nabla)\vec{u} = \frac{\mu}{\rho}\nabla^2\vec{u} - \frac{1}{\rho}\nabla p + \frac{1}{\rho}\vec{F} \tag{8}$$

In equation (8) p denotes the static pressure and μ is the dynamic viscosity of the blood. Also, $\vec{F}$ is the force acting on the fluid particles due to ultrasound. In general, the force component in the acoustic axis direction is more significant than the others. Therefore, in previous studies (Huang, 2002; Solovchuk et al., 2013a), only this component was taken into account. If the z-axis is assumed as the acoustic axis direction, then the streaming force can be calculated based on equation (9). The acoustic intensity (I) in the right-hand side of equation (9) can be obtained from equation (5) (Huang, 2002; Huang et al., 2004).

$$F_z = \frac{2\alpha}{c} I \tag{9}$$

Equation (8) is obtained based on the Newtonian flow assumption. At low values of shear rate (approximately less than 10 s^{-1}), the red blood cells deform and stick together to form reversible aggregates like a stack of coins. The presence of the aggregates can increase the resistance against blood flow and can increase the blood viscosity significantly, and therefore, the non-Newtonian effects should be considered (Fenech et al., 2009; Liu and Liu, 2006; Mehri et al., 2018). In subsequent sections, it will be indicated that in the current specifications, the shear rate of the streaming velocity field is approximately low. Hence, the impact of non-Newtonian blood flow on the streaming profile is also included in the present study. The hemodynamic equation for non-Newtonian flow can be written as follows (Karimi et al., 2014):

$$\frac{\partial \vec{u}}{\partial t} + (\vec{u}\cdot\nabla)\vec{u} = -\frac{1}{\rho}\nabla p - \frac{1}{\rho}\nabla\cdot\tau + \frac{1}{\rho}\vec{F} \tag{10}$$

In this equation, τ is the shear stress and is obtained from equation (11).

$$\tau = \eta(\nabla u + (\nabla u)^T) \tag{11}$$

In this equation, η is the blood flow apparent viscosity, which is a function of strain rate ($\dot{\gamma}$) and can be described by different models. In the present study, power law and Carreau models presented in equations (12) and (13) are used (Karimi et al., 2014). It should be noted that based on the results of Mehri et al. (2018), these two models match well with the experimental results associated with RBC aggregation.

$$\eta(\dot{\gamma}) = k(\dot{\gamma})^{n-1} \quad k = 0.017, n = 0.708 \tag{12}$$

$$\eta(\dot{\gamma}) = \eta_\infty + (\eta_0 - \eta_\infty)\left[1 + (\lambda\dot{\gamma})^2\right]^{(n-1)/2} \quad \eta_\infty = 0.0035\ Pa.s\ , \quad \eta_0 = 0.056\ Pa.s\ ,\ \lambda = 3.313005\ ,\ n = 0.3568 \tag{13}$$

2.3. Temperature model in the liver and the vascular bed

The thermal ablation in tissue comprising microvasculature can be modeled by the Pennes bioheat transfer equation, which is presented in equation (14). In this equation, C, ρ, k and T are the specific heat, density, tissue thermal conductivity and temperature field, respectively. The subscripts t and b refer to the tissue and blood, respectively. Also, w is the perfusion rate of the capillary bed, and T_∞ is the temperature at a distant location from the transducer focus (which is usually 37 °C) (Pennes, 1948).

$$\rho_t C_t \frac{\partial T}{\partial t} = \nabla\cdot(k_t\nabla \mathrm{T}) - w_b C_b (T - T_\infty) + Q \tag{14}$$

The Pennes bioheat equation can be used in domains which include blood vessels with a diameter smaller than 0.5 mm. However, in regions which contain blood vessels with a diameter larger than 0.5 mm, the cooling effect should be considered separately, and homogenization assumption is not valid (Hariharan et al., 2007; Kolios et al., 1995, 1996; Shih et al., 2012; Solovchuk et al., 2013a). Therefore, in these regions, equation (15) can be used to predict the temperature field in the blood vessels. In this equation, $\rho_b C_b \vec{u}\cdot\nabla T$ is related to the convective cooling of vessels and $\vec{u}$ is the blood velocity.

$$\rho_b C_b \frac{\partial T}{\partial t} = \nabla\cdot(k_b\nabla T) - \rho_b C_b \vec{u}\cdot\nabla T + Q \tag{15}$$

In equations (14) and (15), the heat source Q can be calculated based on the equation (6). Hence, the thermal energy equation is coupled with the ultrasound propagation one via this heat source term. Also, the blood velocity can be calculated based on the hemodynamic equation, which is presented in section 2.2. Therefore, HIFU simulation in perfused tissues requires a coupled model of acoustic, thermal, and hemodynamic equations.

Finally, the HIFU effect on cancer cells and the amount of tissue necrosis is calculated according to the thermal dose concept, which was

developed by Sapareto and Dewey (1984). This concept gives a relation between the temperature field in the tissue and the HIFU exposure time required to kill the cancer cells. In HIFU application, the thermal dose can be obtained based on the equation (16). In this equation, R is a parameter which is equal to 2 when T is higher than 43 $^{\circ}C$ and is 4 when T is between and 43 $^{\circ}C$. Also, t_0 and t_{final} are the initial time and final time of treatment, respectively. For calculating the thermal dose, the term R^{T-43} is integrated over the whole treatment time where T is obtained from equations (14) and (15). Based on this definition, the tissue which undergoes necrosis is the region which is surrounded by a surface with thermal dose value of 240 min (Hariharan et al., 2007; Sapareto and Dewey, 1984).

$$TD = \int_{t_0}^{t_{final}} R^{(T-43)} dt \tag{16}$$

2.4. Problem description

In the present study, a 1 MHz single element transducer with a focal length of 10 cm and an aperture diameter of 10 cm is used to deliver the continuous and focused ultrasound waves to the targeted region of the tissue. The schematic configuration for the numerical simulation domain is indicated in Fig. 1 (a). As can be seen, the cylindrical piece of liver is located in a water tank for acoustic impedance matching. The parameters utilized in the numerical model are presented in Table 1. In this table, f_0 is the source frequency.

Since in this study, the effect of vascular bed on HIFU treatment is investigated, the geometry is not axisymmetric because of the presence of the blood vessels. Therefore, a three-dimensional computational domain is defined (Fig. 1 (b)). However, ultrasound propagation modeling requires a refined mesh to capture the wavelength of the ultrasound wave, and the three-dimensional simulation of the acoustic equation results in a substantial computational cost. Therefore, in this study, the simulation of the acoustic pressure field is conducted on a 2D axisymmetric model (Fig. 1 (a)) according to the idea of Huang (2002). This assumption is supported based on the fact that the blood and tissue acoustic impedances are nearly the same, and acoustic scattering does not occur (Hoskins et al., 2010). Hence, the effect of vascular bed on the acoustic field can be neglected, and a 2D axisymmetric model is used to determine the acoustic pressure. In fact, according to Fig. 1 (a), the 2D geometry of the liver is assumed without any blood vessels in the water tank, and since the cylindrical tissue and water tank are coaxial and the focal point is located at the center of the liver, using the 2D axisymmetric model can be justified for pressure field calculations. Then, the 2D acoustic intensity field is mapped from the 2D geometry to the 3D one using predefined functions. Finally, the flow and temperature fields in the 3D liver including blood vessels are obtained.

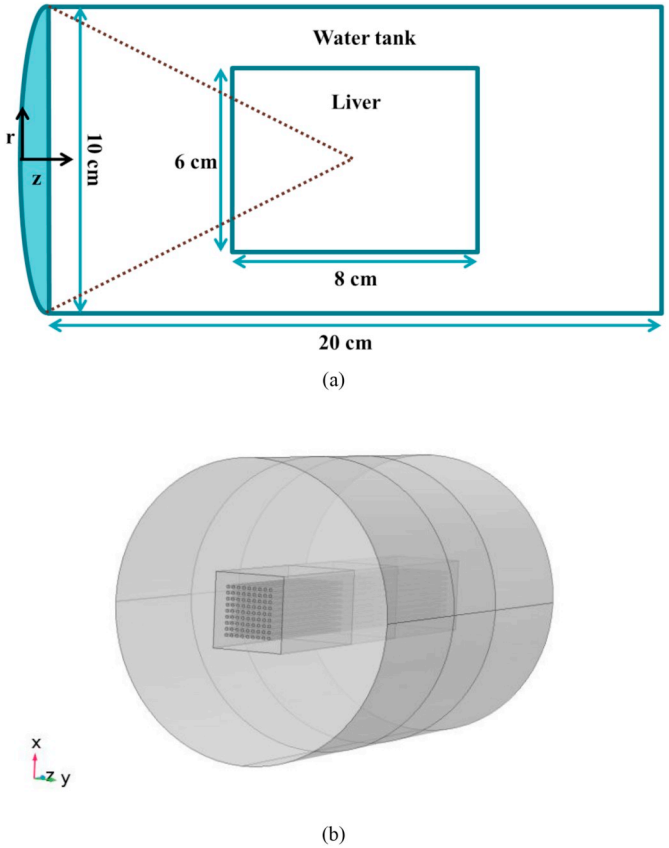

Fig. 1. (a) The 2D domain for the numerical simulation of HIFU exposure to the liver tissue, (b) the 3D computational domain for velocity and temperature fields.

Table 1
Parameters used for the numerical study.

Parameters		
Acoustic Parameters	Frequency (MHz)	1
	aperture diameter (cm)	10
	focal length (cm)	10
	Power (W)	20
	Sonication duration (s)	10
Liver properties	Sound speed (m/s)	1550
	Density (kg/m^3)	1055
	Thermal capacity (J/kg.K)	3600
	Thermal conductivity (W/m.K)	0.512
	Absorption coefficient (Np/m)	$9*f_0$
	Nonlinear coefficient	4.4
Blood properties	Sound speed (m/s)	1540
	Density (kg/m^3)	1060
	Thermal capacity (J/kg.K)	3770
	Thermal conductivity (W/m.K)	0.53
	Absorption coefficient (Np/m)	$1.5*f_0$
	Nonlinear coefficient	4
	Blood perfusion rate (1/s)	0.01
Water properties	Sound speed (m/s)	1482
	Density (kg/m^3)	1000
	Thermal capacity (J/kg.K)	4179
	Thermal conductivity (W/m.K)	0.6374
	Absorption coefficient (Np/m)	0.024983
	Nonlinear coefficient	3.6
Geometrical specifications	Liver diameter (cm)	6
	Liver length (cm)	8
	Water tank length (cm)	20
	Blood vessel diameter (cm)	0.06

In the present study, the vascular bed is considered to be the terminal arterial branches with a diameter of 0.6 mm (Peng et al., 2011). This choice is based on the results of research by Peng et al. (2011). In this research, the cooling effect of different generations of the liver vasculature was examined on thermal ablation by using porous media theory. The results of this study showed that the cooling effect of median vessels such as terminal arterial branches on thermal ablation outcome is considerable.

The 3D computational domain for velocity and temperature fields, which contains a vascular bed with a density of 0.2, is shown in Fig. 1 (b). It is worth noting that thermal and hemodynamic equations are only solved in the liver and vascular bed. Also, it should be noted that since HIFU is a local thermal ablation procedure which affects the tissue in a small region, the density of the vascular bed introduced in this study is the local density and is calculated based on the accumulation of blood vessels near the focal zone. As can be seen in Fig. 1 (b), the vascular bed is constructed from parallel terminal arterial branches, which are uniformly distributed in the liver. The number of the vessels in the liver is calculated based on the assumed local density, and then, they are evenly located in the liver parallel to the acoustic axis. The reason for assuming a vascular bed, which is parallel to the acoustic axis, is based on the

results of the study by Solovchuk et al. (2013a). In their study, it was shown that the cooling effect of a vessel which is in the direction of the acoustic axis is more pronounced on the HIFU efficacy than the perpendicular blood vessel. Also, it should be noted that the assumed simple geometry of the vascular bed is not the realistic configuration of the vasculature in the liver. However, it can be a starting point to consider the effect of vascular bed on temperature distribution and lesion size in a perfused tissue such as liver with a lower computational cost compared to the case of modeling the real geometry of the vascular bed.

In acoustic pressure field calculations, a source pressure is calculated based on equation (4) and assigned to the transducer surface. Also, the computational domain is truncated by the perfectly matched layers (external surfaces of the water tank in Fig. 1(a)) to absorb the acoustic waves and to avoid reflection. Furthermore, an axial symmetry boundary condition is applied at $r = 0$. In the hemodynamic calculations, uniform velocity and constant pressure boundary conditions are used at the inlet and outlet of the blood vessels, respectively. Also, a no-slip boundary condition is assigned to the vessel walls. In heat transfer simulations, all of the liver lateral surface temperatures are assumed to be equal with the body temperature ($37\ ^{\circ}C$). Besides, a fixed temperature boundary condition of $37\ ^{\circ}C$ is considered at the inlet of the vascular bed as well as the tissue, and a zero gradient temperature boundary condition (open boundary condition) is assigned to the outlet surfaces. Temperature and heat flux continuity is also imposed at the blood vessels walls. The initial temperature of the tissue and blood is assumed to be $37\ ^{\circ}C$ as well.

2.5. Simulation model

The numerical procedure is briefly described in this section. Firstly, the acoustic pressure in the two-dimensional domain is obtained based on the linear Westervelt equation in the frequency domain for assumed transducer specifications. Then, the 2D acoustic intensity field is calculated from equation (5) and is mapped from the 2D geometry to the 3D one by using mapping functions to calculate the power deposition and acoustic streaming force using equations (6) and (9), respectively. In the next step, the acoustic streaming velocity profile in the vessels is calculated by the hemodynamic equations along with the term related to the acoustic streaming phenomenon. Based on our calculations, blood velocity reaches the steady-state condition in a short time (approximately 0.2 s) compared to the whole treatment time. Therefore, the steady-state velocity profile is calculated once and is used as the input to the transient heat transfer calculations. With the known ultrasound deposition and blood velocity profile, the bioheat and energy equations in tissue and blood (equation (14) and (15)) are solved, and the temperature field is calculated. The time step used for simulation is chosen 0.025 s. It should be noted that based on the considerations, this time step is small enough to have an accurate thermal simulation. Finally, the lesion size can be calculated based on the transient temperature field.

The two-dimensional acoustic equation, three-dimensional hemodynamic and heat transfer equations along with initial and boundary conditions are solved by utilizing the finite element method via COMSOL Multiphysics 5.3 (Pressure Acoustics Frequency Domain, Laminar Flow, Bioheat Transfer; Comsol, Inc.; Burlington, MA; USA). For acoustic pressure, the analysis is conducted in the axisymmetric two-dimensional computational domain (Fig. 1 (a)). For this analysis, the FEM model is discretized using elements with the Lagrange quartic shape functions. A maximum mesh size of $\lambda/6$ (λ is the wavelength) in the focal region and a maximum mesh size of $\lambda/4$ in the rest of the domain is used for grid generation. The number of elements generated for acoustic pressure calculation is approximately 150000. Finally, the system of governing equations along with initial and boundary conditions are solved using MUMPS solver to obtain the acoustic pressure field. In the analysis of velocity and temperature fields, elements with the Lagrange linear shape functions are used. For grid generation in the focal region, the refined grid is generated with a maximum element size of $\lambda/3$. The number of elements used for velocity and temperature calculations is varied from 500000 to 700000 for different values of vascular density. The system of governing equations along with initial and boundary conditions for the velocity and temperature fields are solved by using MUMPS and GMRES solvers, respectively.

The mesh independence study, which is conducted for the acoustic pressure field, is presented in Table 2. According to this table, by mesh refinement in mesh 3 compared to mesh 2, only 0.0874% difference in focal intensity is observed. Hence, to reduce the computational cost, mesh 2 with a maximum element size of $\lambda/4$ is used in the calculations. The sensitivity analysis of focal temperature to the grid size used in heat transfer calculation is presented in Table 3. It should be noted that this sensitivity analysis is conducted on the two-dimensional domain and then is generalized for the three-dimensional one. As can be seen, the temperature field is less sensitive to the grid size used for calculations.

3. Results

3.1. Model validation

Our numerical model is verified by comparing the obtained results with the ones of Solovchuk et al. (2013a) and Hariharan et al. (2007). First of all, the value of acoustic pressure and intensity obtained at the focal point is verified by comparing with the numerical results of Solovchuk et al. (2013a) as demonstrated in Table 4. In this case, the ultrasound waves with the energy of 80 W and the frequency of 1 MHz are emitted from a source and propagate in the liver toward the targeted region. The spherically focused transducer used in this study has an aperture radius of 6 cm and a focal length of 12 cm. Because of the symmetric geometry used in this study, the acoustic propagation is simulated based on a 2D axially symmetric model. It is observed that the difference between the obtained values of these two studies is less than 0.5%.

Next, the heat deposition due to the generated acoustic field (with the focal intensity of 327 W/cm^2) is calculated, and the energy equation is solved to obtain the temperature field. In Fig. 2, the temperature distributions along the x-direction in the case of no blood flow at $t = 8$ s and $t = 20$ s are compared to those of Solovchuk et al. (2013a). In this case, the liver is exposed to HIFU for 8 s. As can be seen, a good agreement is obtained, and the difference is less than 0.5%. The results for no blood flow case are also validated by the numerical and experimental results of Hariharan et al. (2007) according to Fig. 3. In this study (Hariharan et al. (2007)), experiments and the corresponding numerical calculations were performed in a phantom which was exposed for 20 s to ultrasound waves with the frequency of 1.5 MHz and the power of 32 W. The aperture radius and the focal length of the transducer used in their study were 5 cm and 15 cm respectively. The cylindrical phantom was located in a water tank, and its axis was coaxial with the transducer which was placed 11 cm from the phantom surface. It is observed that the transient temperature rise obtained in the present study agrees well with the numerical results of Hariharan et al. (2007) and agrees within 10% with their experimental results in the validation phantom.

For validating the coupled set of acoustics, thermal, and fluid models, the temperature distribution along x-direction at $t = 8$ s is compared to the numerical result of Solovchuk et al. (2013a) according to Fig. 4. In this case, a 3 mm diameter blood vessel parallel to the

Table 2
Mesh independence study for acoustic pressure calculation.

Mesh	Maximum element size	Number of elements	Focal acoustic intensity	Difference (%)
1	$\lambda/2$	34728	351.850	–
2	$\lambda/4$	138759	357.029	1.472
3	$\lambda/6$	314977	357.341	0.0874

Table 3
Mesh independence study for heat transfer calculation.

Mesh	Maximum element size (mm)	Number of elements (2D domain)	Focal temperature	Difference (%)
1	4	4770	88.95	–
2	2	16950	88.908	0.047%
3	1	61876	88.906	0.0022%

Table 4
Comparison of focal pressure and intensity with the results of Solovchuk et al. (2013a).

	Solovchuk et al.	Present study	Difference
focal pressure	3.27 MPa	3.26 MPa	0.3%
focal intensity	327 W/cm^2	326.5 W/cm^2	0.15%

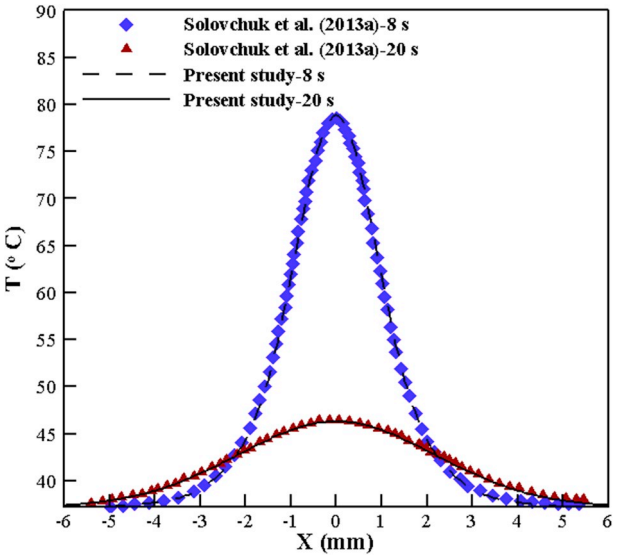

Fig. 2. Temperature distribution along x-direction at 8 s and 20 s obtained from the present study and the study of Solovchuk et al. [4] for no blood flow case.

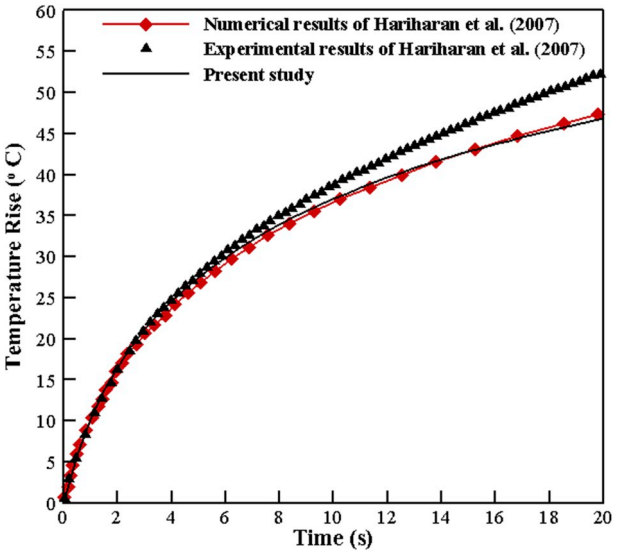

Fig. 3. Comparison of the transient temperature rise obtained in the present study with the numerical and experimental results of Hariharan et al. [21] in a validation phantom at the power of 32 W.

acoustic axis is considered and the distance between the vessel wall and the focal point is taken to be 1 mm. It can be seen that a good agreement is obtained and the difference between the two models is less than 0.5%.

Finally, for streaming model validation, the streaming profile in a 3 mm diameter blood vessel is obtained at the focal plane and is compared with the one of Solovchuk et al. (2013a) in Fig. 5. In this figure, the results are presented for two distances between the blood vessel center and the focal point (focal point is located at the blood vessel center or blood vessel wall). It can be observed that the streaming profiles calculated in the present study are in good agreement with the streaming profiles obtained in the study of Solovchuk et al. (2013a).

3.2. Temperature distribution in a tumor located within a vascular bed

In this section, the effect of a bed comprising terminal arterial branches on the temperature distribution due to HIFU exposure is studied. The terminal arterial branch is a vascular generation which contains 0.6 mm diameter blood vessels with 6.55 cm/s average blood flow velocity (Peng et al., 2011). The effect of the vascular density ($\varepsilon = 0.05,\ 0.1,\ 0.2$) is also investigated on the obtained results. The vascular density affects the distance of the blood vessels from the focal point and the number of them around the focal region. The spacing between the focal point and the nearest blood vessel wall for different vascular densities is presented in Table 5. A single vessel is also considered at three different distances given in Table 5, to compare its cooling effect with the corresponding vascular bed.

In Fig. 6, the computed temperature contours at the cutting planes $z = 10$ cm and $y = 0$ at $t = 10$ s for the cases of no blood flow, single vessel at the distance of 0.8769 mm from the focal point and the vascular bed with a density of 0.2 are presented. In Fig. 6(a) & d, it can be observed that a symmetric high-temperature region with an ellipsoidal shape is formed. Also, it can be seen that in the presence of a single vessel (Fig. 6(b) & e) the temperature contour becomes axisymmetric and shifts towards the region with the less cooling effect. Moreover, when the tumor is located within a vascular bed (Fig. 6(c) & f); the high-temperature area is enclosed by nearby blood vessels. Since the vascular bed considered in the present study is symmetric, the temperature contour is also symmetric. It is observed that the maximum temperature at the focal point in the presence of vascular bed is reduced considerably in comparison to the no blood flow case and in the presence of single vessel.

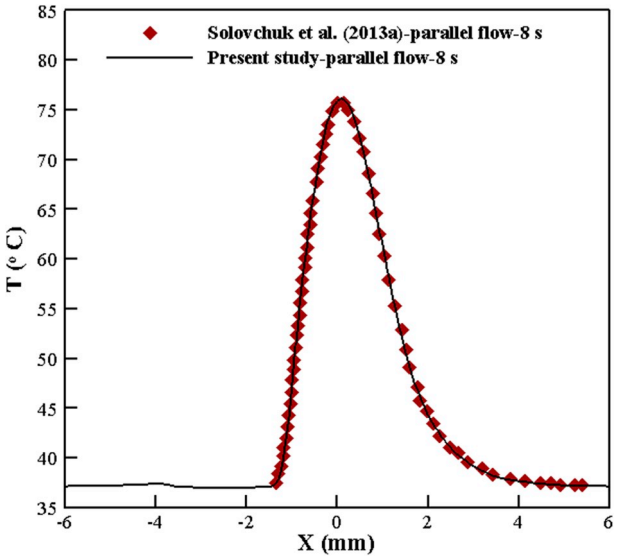

Fig. 4. Temperature distribution along x-direction at t = 8 s obtained from the present study and the study of Solovchuk et al. [4] when a 3 mm diameter blood vessel is present.

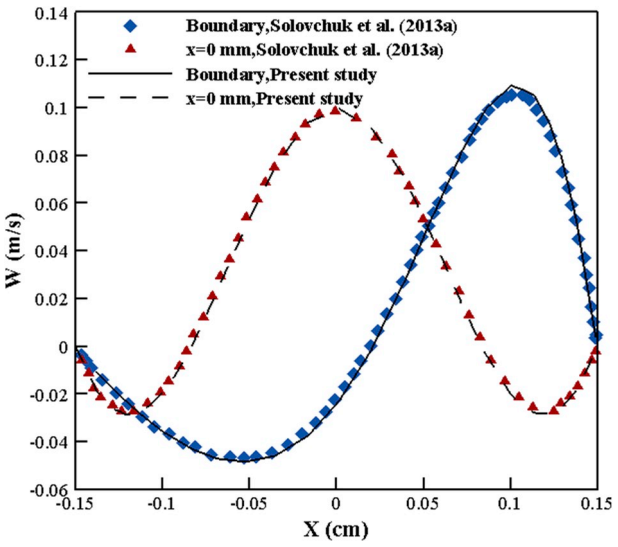

Fig. 5. The streaming profile in the z-direction obtained from the present study and the study of Solovchuk et al. [4] for two distances between focal point and blood vessel center.

Table 5
The distance of the focal point from the wall of the nearest blood vessel.

Vascular density (ε)	The distance of the focal point from the wall of the nearest blood vessel (mm)
0.05	1.89
0.1	1.23
0.2	0.8769

The temperature contours at the cutting planes $z = 10$ cm and $y = 0$ in the presence of vascular bed with different vascular densities are presented in Fig. 7. It can be seen that an ellipsoidal shape high-temperature area is formed between the vessels, and increasing the vascular density reduces the extent of this region, and results in lower values of temperature in the focal region. Also, it is evident that only the convective cooling effect of nearby vessels affects the extent of the high-temperature zone.

In Fig. 8, the temperature distributions at t = 10 s along the *x*-axis and the *z*-axis, are presented for the case of no blood flow and the vascular bed with different densities. At $t = 10$s, the peak temperature is 88.9 °*C* in the absence of blood flow. However, in the presence of vascular bed with a density of 0.05, 0.1, and 0.2, the peak temperature reduces to 88.2 °*C*, 82.7 °*C*, and 71.8 °*C* respectively. Also, according to Fig. 8(a), for the assumed geometry of vascular bed, the extent of the high-temperature region in the *x*-direction is narrowed by increasing the vascular density. But according to Fig. 8(b), the vascular density has a negligible effect on the extent of the high-temperature region in the *z*-direction. This statement is limited to the assumed geometry of the vascular bed.

The variations of focal temperature with time for cases of no blood flow, single vessel at different distances from the focal point, and vascular beds with different densities are presented in Fig. 9. For the vascular bed with a density of 0.05 (Fig. 9(a)), the cooling effect is minor and the difference is only apparent in the cooling phase of the treatment. However, it can be observed that the vascular beds with a density of 0.1 and 0.2 have a considerable cooling effect on the focal temperature in comparison to the no blood flow case and the single vessel which is located at the same distance from the focal point.

3.3. Acoustic streaming effect on velocity profile in the terminal arterial branches

In this section, the acoustic streaming profile in terminal arterial branches is considered. First of all, the generated velocity profile in terminal arterial branches (with $U_{inlet} = 0$) is investigated when the blood vessel center and the focal point coincide. In Fig. 10 (a) the induced streaming profile in the blood vessel is indicated. Based on this figure, the maximum shear rate in the Newtonian case can be calculated,

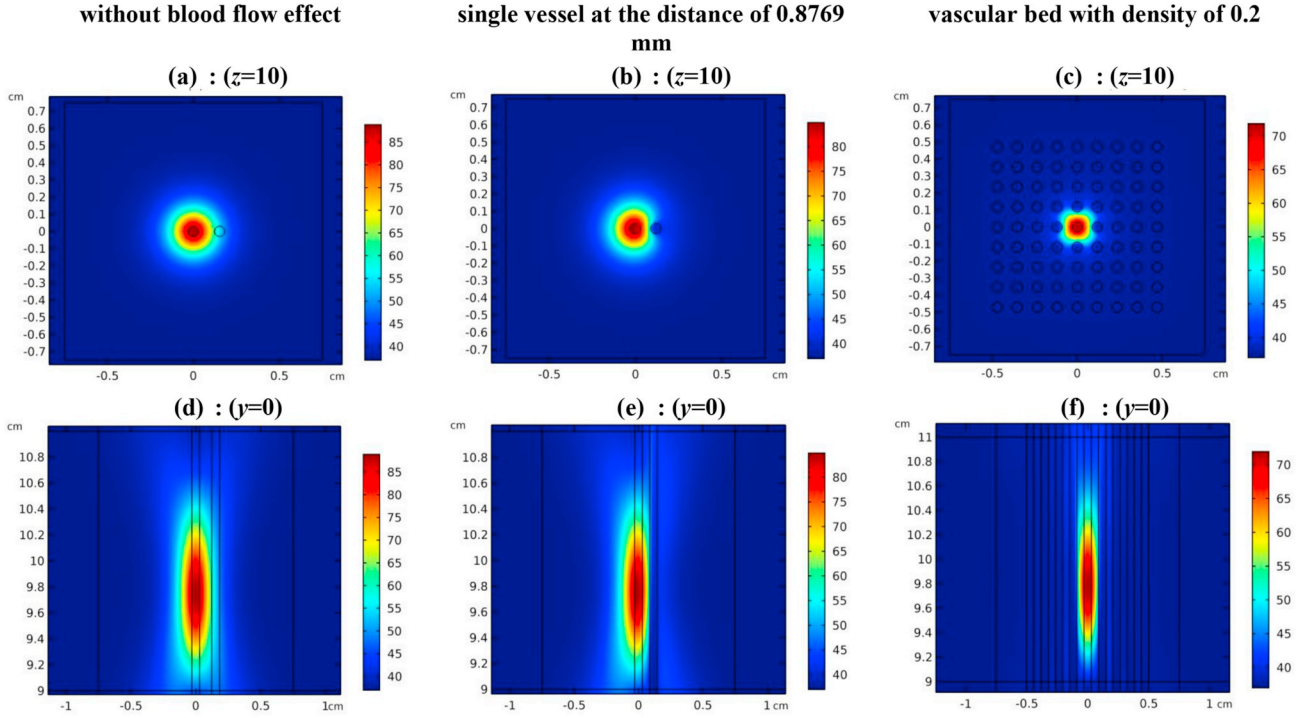

Fig. 6. The calculated temperature contours at t = 10 s at the cutting planes z = 10 cm (a,b,c) and y = 0 (d,e,f). (a,d) without blood flow effect, (b,e) in the presence of a single vessel at the distance of 0.8769 mm from the focal point, (c,f) in the presence of vascular bed with a density of 0.2.

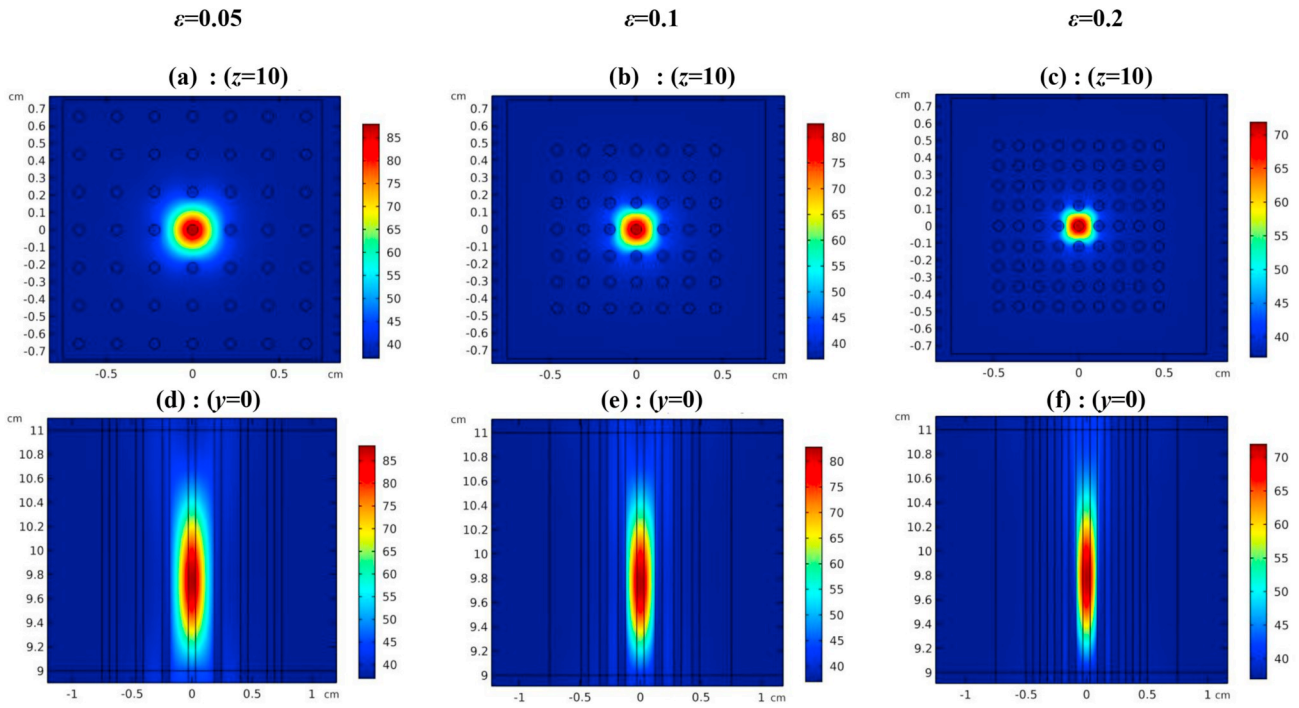

Fig. 7. The calculated temperature contours at t = 10 s at the cutting planes z = 10 cm (a,b,c) and y = 0 (d,e,f). (a,d) vascular bed with a density of 0.05, (b,e) vascular bed with a density of 0.1, (c,f) vascular bed with a density of 0.2.

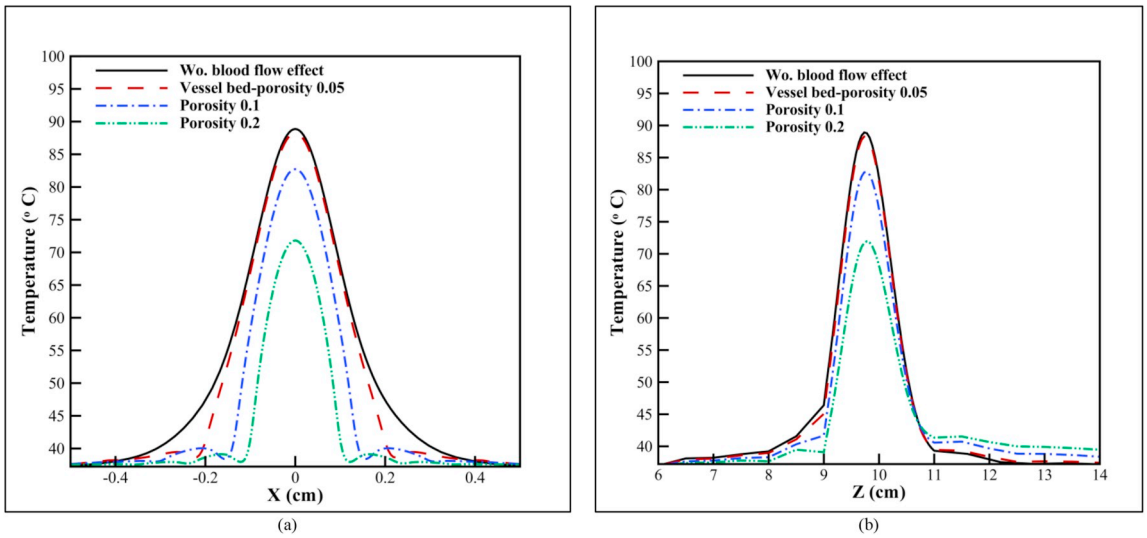

Fig. 8. The temperature distributions at t = 10s along (a) x-axis and (b) z-axis for cases of no blood flow and in the presence of vascular bed with different vascular densities.

which is about 4 s^{-1}. This value of shear rate is approximately low, and according to the results of Mehri et al. (2018), the non-Newtonian effects become important. Therefore, in Fig. 10 (a) the predicted acoustic streaming profiles with different non-Newtonian flow assumptions are also indicated. According to this figure, the maximum value of the generated velocity profile for Newtonian flow is small. This result is in agreement with the results of Solovchuk et al. (2013a). In fact, the peak streaming velocity increases with blood vessel diameter (Solovchuk et al., 2013a), and due to the small diameter of the terminal arterial branches, the induced acoustic streaming field is weak. Moreover, it can be seen that the non-Newtonian behavior of blood flow decreases the peak streaming velocity in the blood vessel as well. Also in Fig. 10(b), the velocity profile in a terminal arterial branch with $U_{inlet} = 6.55$ cm/s in the absence of acoustic streaming is compared to the velocity profile in the presence of this effect. In this case, the distance between the focal point and the blood vessel wall is 0.8769 mm. As can be seen, the acoustic streaming has no effect on the velocity field in the blood vessel.

3.4. Effect of vascular density (amount of tissue vascular content) on lesion size

In Table 6, the volume of lesion created by HIFU exposure for different cases is presented. The lesion volume in the presence of vascular bed with the density of 0.05, 0.1, and 0.2 is decreased by an amount of 15.5%, 55.4%, and 78.6% respectively in comparison to the no blood flow case. Also, in Fig. 11, the thermal dose contours for the

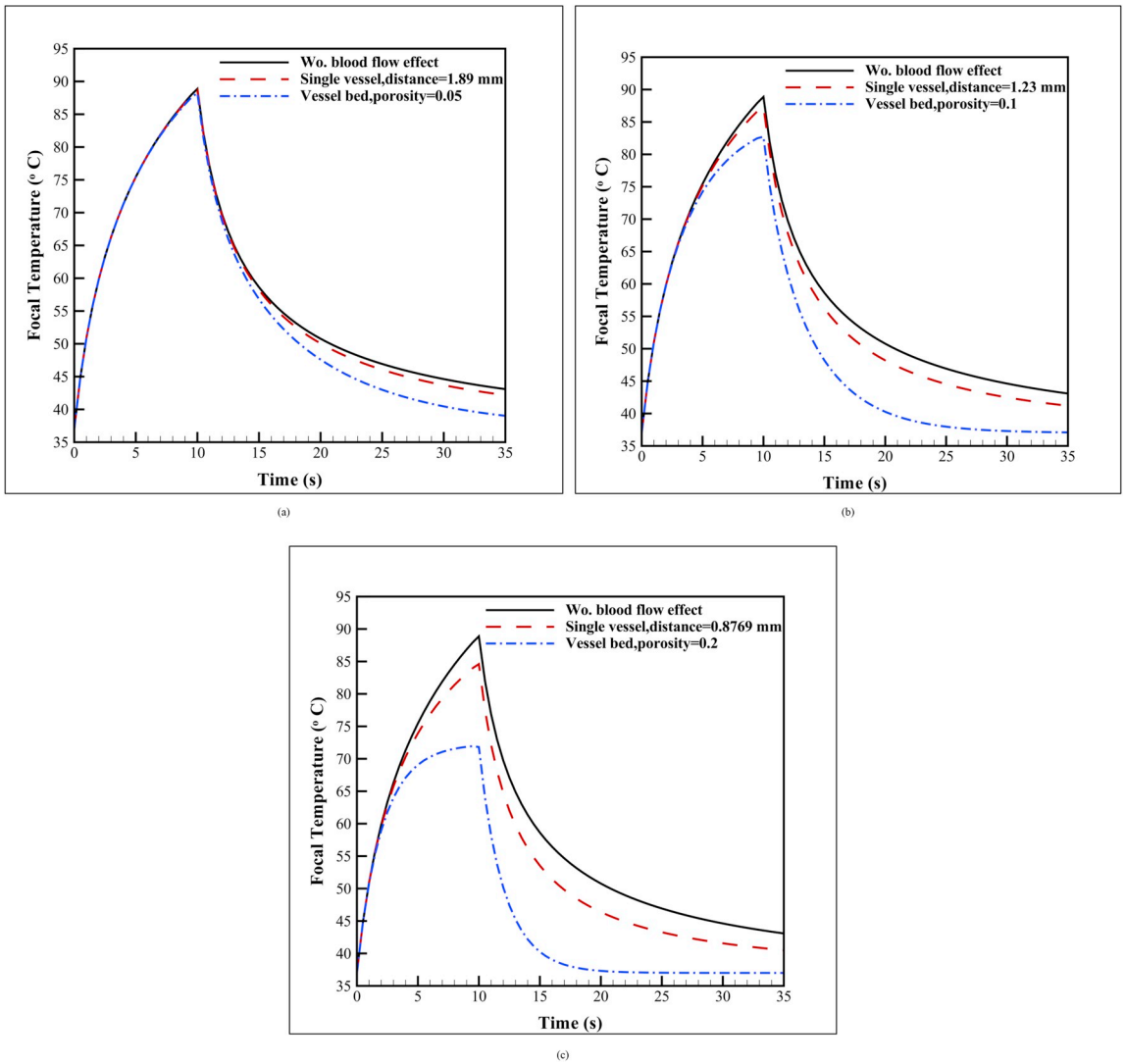

Fig. 9. Variation of focal temperature with time for different cases of no blood flow and in the presence of a single vessel and vascular bed; (a) vascular bed with the density of 0.05 and single vessel with the same distance, (b) vascular bed with the density of 0.1 and single vessel with the same distance, (c) vascular bed with the density of 0.2 and single vessel with the same distance.

condition of no blood flow and in the presence of the vascular bed with different densities are indicated. In this figure, the area inside the red line is the thermal lesion, which is related to the region heated for more than 240 min at 43 $^{\circ}C$. It is indicated that the cooling effect of vascular bed reduces the lesion size in radial and axial directions. For example, the lesion sizes obtained in the absence of the blood vessel are 3.1 mm and 12.9 mm in the radial and axial directions, respectively. However, for the vascular bed with a density of 0.2, the lesion sizes in the radial and axial directions are 1.5 mm and 10.3 mm. As can be seen, in the presence of the vascular bed of simple geometry with a density of 0.1 and 0.2, the region close to the blood vessel wall remains viable.

One of the main concerns in HIFU application in the vascular bed is the ability of HIFU to ablate the region between blood vessels effectively. For this investigation, first, the maximum lesion size in the z-direction (acoustic axis direction) in the cutting plane *XZ* versus vascular density is indicated in Fig. 12. It can be observed that in the presence of vascular bed with the density of 0.05, 0.1, and 0.2 the maximum lesion size in the z-direction is reduced by the amount of 2.5%, 8.3%, and 21% respectively in comparison to the no blood flow case. Also, another essential factor which can show the effectiveness of HIFU in ablation of the region between the blood vessels is the ratio of the maximum lesion size in the x-direction (perpendicular to the acoustic axis direction) to the distance between the two neighbor blood vessels. For the vascular bed with a density of 0.1 and 0.2, this ratio is calculated to be 0.87 and 0.86, respectively. Therefore, at least approximately 14% of the cancer cells remain viable near the blood vessel walls. It is interesting to note that this ratio is almost unchanged by variation of the vascular density. Again, it is worth noting that these concluding remarks are limited to the idealized geometry considered in the present study.

3.5. Solutions to improve HIFU efficacy for ablation of tumor in the vascular bed

According to section 3.4, it seems that HIFU doesn't work effectively in the vascular bed with high density and regions near the blood vessels walls remain viable. Therefore, there is a tendency to propose some solutions to improve HIFU efficacy in perfused tissues. To overcome the cooling effect of the vascular bed, the HIFU heat deposition should be increased. According to equation (6), the HIFU heat deposition is proportional to intensity and absorption coefficient. Also, according to equation (5), the intensity is proportional to the acoustic pressure squared. Hence, the focal pressure and absorption coefficient of the tumor should be adjusted to increase the HIFU heat deposition. The absorption coefficient of the tumor is enhanced by increasing the

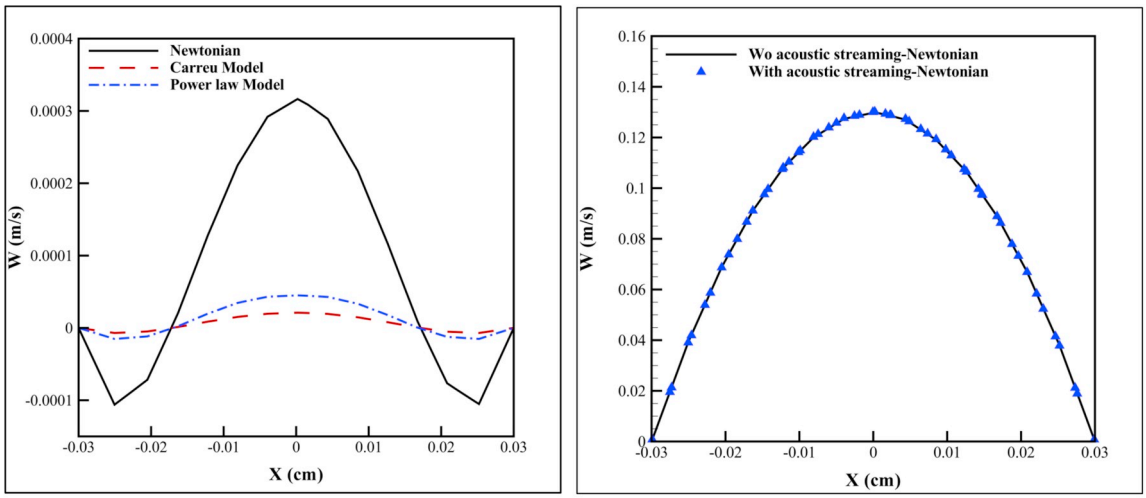

(a) (b)

Fig. 10. (a) generated acoustic streaming profile in the z-direction in the terminal arterial branches when the focal point and blood vessel center coincide($U_{inlet} = 0$); (b) blood velocity in the z-direction in the terminal arterial branches with $U_{inlet} = 6.55$ cm/s and for the distance between the blood vessel wall and the focal point of 0.8769 mm.

Table 6
Lesion volume for the cases of no blood flow, single vessel at different distances from the focal point, vascular bed with different vascular densities.

Different cases	Lesion volume (mm^3)
Wo. Blood flow effect	69.1
Single vessel, Distance = 1.89 mm	66.32
Single vessel, Distance = 1.23 mm	58.9
Single vessel, Distance = 0.8769 mm	51.3
Vascular bed, $\varepsilon = 0.05$	58.4
Vascular bed, $\varepsilon = 0.1$	30.8
Vascular bed, $\varepsilon = 0.2$	14.8

frequency of the transducer. It is worth noting that by increasing the frequency, the attenuation coefficient of the intervening tissue is also increased and the acoustic waves are more attenuated during propagation to the focal region. Focal pressure (p_F) is obtained based on equation (17) in terms of transducer pressure and transducer Gain (Hariharan et al., 2007). In this equation, a is the aperture radius of the transducer. Therefore, increasing source pressure or angular frequency or aperture radius of the transducer can increase the focal pressure. Also, due to the conduction from the focal region to the peripheral region, it is expected that by increasing the treatment time of the HIFU, the conduction takes place more effective and this increases the lesion volume. Hence, in this section, the results of increasing the source pressure, angular frequency, aperture radius, and treatment time are presented and compared to each other.

$$\frac{p_F}{p_0} = \frac{\omega a^2}{2c_0 d} = Transducer\ Gain \tag{17}$$

It is worth noting that the parameters of equation (17) are increased in a way that the focal pressure enhanced by the amount of approximately 20%. Also, the treatment time is increased by the amount of 50%. In Table 7, the maximum lesion sizes in the x-direction and the z-direction and the ratio of the maximum lesion size in the x-direction to the distance of two neighbor vessels (which is named the ablation efficacy ratio in the rest of the manuscript) for different cases are presented. According to Table 7, by increasing the source pressure by the amount of 20% the ablation efficacy ratio increases 13% and only 0.3% of the cancer cells near blood vessel walls remain viable. Also, it is observed that in this case, the lesion size in the z-direction is approximately equal to the lesion size for the no blood flow case. Moreover, by increasing the frequency and the aperture radius by the amount of 20% and 10%, the ablation efficacy ratio is increased by 6% and 10%, respectively. Also, in both cases, the lesion size in the z-direction is reduced slightly. The heat deposition along the z-axis (acoustic axis) for different cases is presented in Fig. 13. It can be observed that increasing the source pressure results in more heat deposition in the intervening tissues. However, by increasing the transducer gain (increasing the transducer radius or frequency), the region with high heat deposition becomes narrower and is limited to the focal zone, and thus the intervening tissues experience lower heat deposition in comparison to other cases. In the last row of Table 7, it is observed that by increasing the treatment time by the amount of 50%, the ablation efficacy ratio is increased 4% and the lesion size in the z-direction is increased slightly.

4. Discussion

In the present numerical study, the considerable cooling effect of liver vasculature on the HIFU ablation efficacy is indicated. It was demonstrated that modeling the convective cooling of vascular bed by using simplified Pennes Bioheat equation results in huge inaccuracies in HIFU treatment planning.

It is shown that in the presence of the vascular bed, the high-temperature region is narrowed by the nearby vessels and the lesion size in the axial and radial directions is reduced. The cooling effect of the assumed vascular bed is considerable that the peak temperature is decreased in comparison to the no blood flow case. Also, it is indicated that the vascular density has a significant effect on the maximum temperature obtained due to the HIFU exposure and the extent of the high-temperature region. This fact is due to the more blood passing around the focal zone and the reduced distance of the nearby blood vessels from the focal point. For the vascular bed with the density of 0.05, the large spacing between the focal point and the nearby vessels, results in negligible cooling effect in the heating phase of the treatment (Fig. 9(a)). However, for the vascular bed of high densities, the cooling effect is so strong that it prevents the temperature rise in the focal region before the termination of the treatment time. One interesting thing which can be observed in Fig. 9(c) is that for the vascular density of 0.2, the cooling effect is so strong such that the focal temperature reaches its steady-state value in approximately 7.5 s. Hence, it seems that HIFU exposure for the duration of 7.5 s is sufficient to increase the focal region temperature to the maximum obtainable value in this condition. This investigation would be an important factor in HIFU treatment planning to ablate the

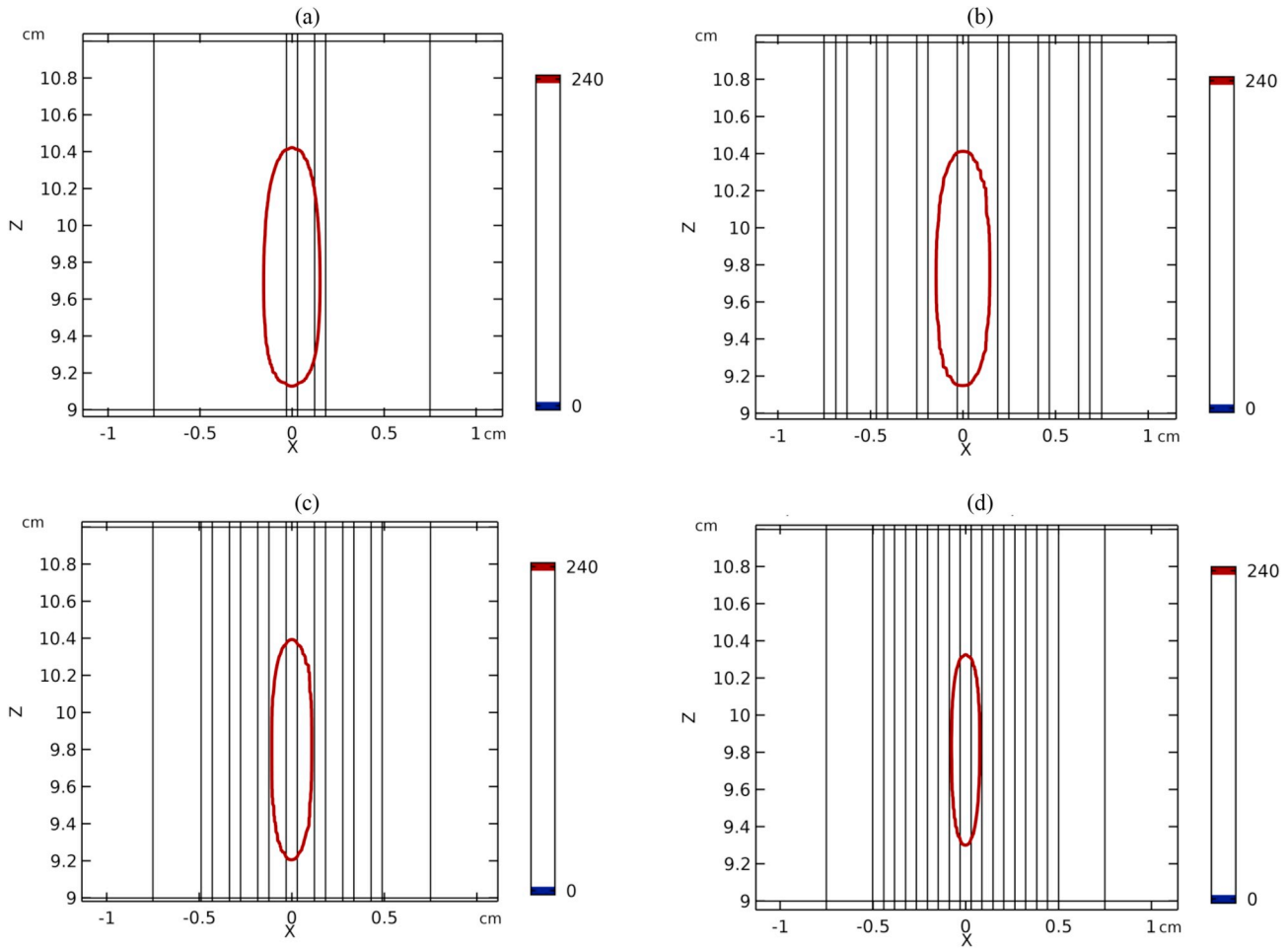

Fig. 11. Thermal dose contour for different cases: (a) without blood flow effect, (b) vascular bed with a density of 0.05, (c) vascular bed with a density of 0.1, (d) vascular bed with a density of 0.2.

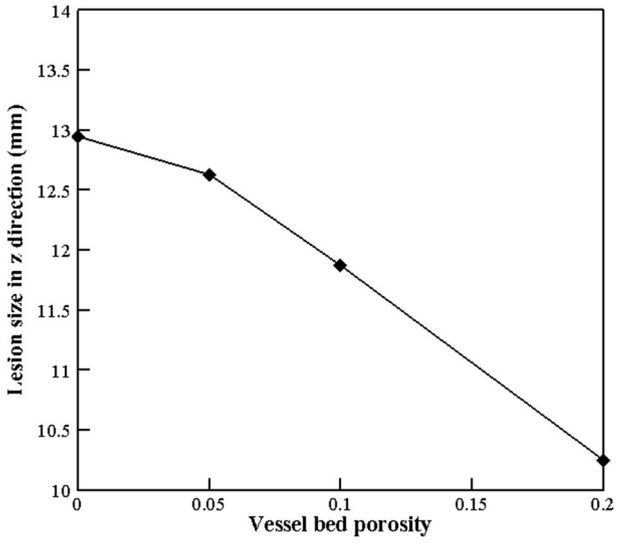

Fig. 12. Lesion sizes in the z-direction versus vascular density.

focal region effectively without damaging intervening tissue.

Moreover, since HIFU is a local ablation procedure, only the convective cooling of nearby vessels affects the extent of the high-temperature region. Therefore, in actual applications, it is sufficient to consider the density and condition of the adjacent vessels around the focal zone. The acoustic streaming phenomenon is also investigated in the vascular bed. It is shown that in vascular beds, including the small diameter blood vessels such as arterial and terminal arterial branches, the acoustic streaming is not an important factor in the cooling effect of the bed.

It is demonstrated that in the presence of the liver vasculature, the lesion size is reduced considerably. Hence, it seems that some cancerous cells remain viable and if multiple ablation points are needed to cover the entire region between the blood vessels, the number of ablation points should be increased considerably with increasing the vascular density, and this increases the treatment time. Therefore, some

Table 7
Maximum lesion size in the x and z-directions and the ratio of lesion size in the x-direction to the distance of neighboring vessels for different cases.

Different cases	Maximum lesion size in x direction (mm)	ratio	Maximum lesion size in z direction (mm)
Wo. Blood flow effect	3.06	–	12.94
Vascular bed, $\varepsilon = 0.2$	1.52	0.868	10.25
Vascular bed, $\varepsilon = 0.2$, $p_0 = p_0{}^*1.2$	1.74	0.997	12.63
Vascular bed, $\varepsilon = 0.2$, $f_0 = f_0{}^*1.2$	1.63	0.929	9.93
Vascular bed, $\varepsilon = 0.2$, $a = a^*(1.2)^{0.5}$	1.69	0.966	10.07
Vascular bed, $\varepsilon = 0.2$, treatment time = 15 s	1.59	0.908	10.75

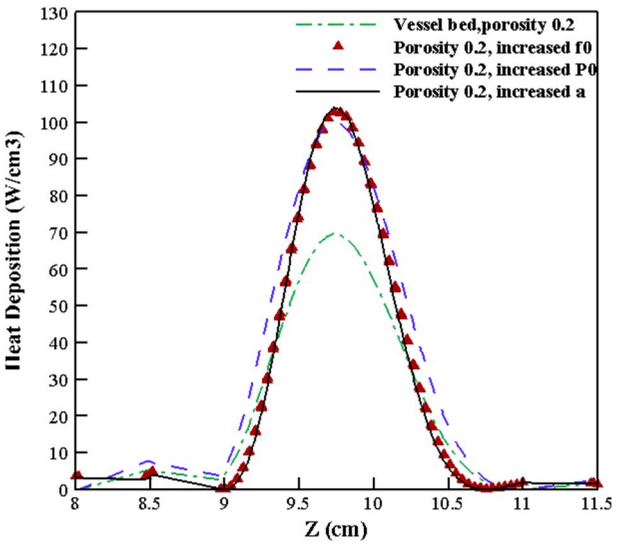

Fig. 13. Heat deposition variation along the *z*-axis (along the acoustic axis) for different cases.

approaches are proposed to compensate for the considerable cooling effect of the liver vasculature and to ablate the cancerous liver region effectively. The first one is to increase the source pressure. Based on the obtained results, it seems that by increasing the source pressure by the amount of 20% the tumor in the vascular bed with a density of 0.2 can be ablated effectively. However, by considering the heat deposition along the acoustic axis direction (Fig. 13), it can be concluded that one of the drawbacks of increasing the source pressure is that the pressure field in the intervening tissues is also increased and this may result in skin burning and injuries to the healthy tissues. In fact, based on the previous studies, it can be said that one of the common complications associated with HIFU therapy is skin burns of various grades (Cheung et al., 2012; Li et al., 2009). Therefore, other approaches (increasing transducer angular frequency or aperture radius) to increase the transducer gain are considered. Based on the obtained results for the vascular bed of idealized geometry, it seems that increasing the aperture radius works more effective than increasing the transducer frequency. Moreover, in Fig. 13, it is indicated that by increasing the transducer gain, the complications related to skin burns and injuries to the healthy tissue do not occur. Hence, it can be concluded that increasing the transducer gain is more preferred for ablating the tumor embedded in the assumed idealized vascular bed when some concerns related to skin burns and healthy tissues are present. The final method to improve HIFU efficacy includes increasing the treatment time. It is indicated that this method results in a minor increase in the lesion size. This increase is due to the conduction effects from the focal region to the peripheral zone. However, increasing the treatment time may result in skin burns and inconvenience for the patient, and this approach is not preferred for increasing the lesion size.

It is worth noting that these conclusions are based on the vascular bed of idealized geometry investigated in the present study and the detailed parameter study on the vascular bed of real geometry will be included in the future research. Also, one of the concerns in HIFU ablation of the liver tumor is the presence of the ribcage in the ultrasound propagation path. Since the presence of the rib bone may cause significant absorption and reflection of the ultrasound waves, the bone and its surrounding tissue may be overheated, and this can result in skin burns (Gelat et al., 2014). Therefore, it is essential to have an optimized focusing scheme to decrease the ultrasound intensity on the ribs by using multi-element transducers. This issue is the focus of some previous researches such as Gelat et al. (2014). Hence, the present study can be extended to propose some focusing approaches by using multi-element transducers to decrease the ultrasound intensity on the ribs and at the same time to ablate the tumor located in the vascular bed efficiently.

5. Conclusion

In this study, combined two-dimensional and three-dimensional models are presented to investigate the effect of the vascular bed of simple geometry comprising terminal arterial branches and its density on the temperature distribution in a liver tumor exposed to HIFU. In the presented model convective cooling of terminal arterial branches is taken into account. It seems that the vascular bed with high density has a considerable effect on temperature variation in the focal region during the treatment time and the cooling effect is so strong such that the steady state condition is reached before termination of the treatment time. It is also demonstrated that in small diameter vessels such as terminal arterial branches, the effect of acoustic streaming is not considerable, and the density of the vascular bed plays the primary role in the cooling effect. It is shown that in the vascular bed with high density, the lesion volume reduces considerably.

It is proposed that in the simple geometry vascular bed investigated, the ratio of the maximum lesion size perpendicular to the acoustic axis direction to the distance of neighboring vessels is a good indicator of the HIFU efficacy in ablating the cancerous region between blood vessels. Based on the obtained values for this ratio, it is indicated that in the current HIFU settings and for the considered vascular bed, approximately 14% of the cancer cells close to blood vessels walls remain viable for the densities of 0.1 and 0.2. Also, it seems that by increasing the accumulation of the vascular bed, the lesion size parallel to the acoustic axis direction is reduced and it causes increasing the treatment time to ablate the whole region between blood vessels. Besides, some solutions are proposed to increase the lesion size in the vascular bed with high density. These solutions include increasing the source pressure or transducer gain. Based on the obtained results, it can be concluded that increasing the transducer gain is more preferred than increasing the source pressure for ablating the tumor embedded in the vascular bed when some concerns related to skin burns and healthy tissue injuries are present. It should be noted that these results are obtained in the case of linear ultrasound propagation, in the absence of relaxation effects, for a single element transducer (not a phased array system) and the vascular bed of idealized geometry. All of these factors affect the treatment algorithm planning and will be considered in our future study.

Funding

This research did not receive any specific grant from funding agencies in the public, commercial, or not-for-profit sectors.

Declaration of competing interest

The authors declare no competing or financial interests.

References

Al-Bataineh, O., Jenne, J., Huber, P., 2012. Clinical and future applications of high intensity focused ultrasound in cancer. Cancer Treat Rev. 38 (5), 346–353. https://doi.org/10.1016/j.ctrv.2011.08.004.

Bailey, M.R., Khokhlova, V.A., Sapozhnikov, O.A., Kargl, S.G., Crum, L.A., 2003. Physical mechanisms of the therapeutic effect of ultrasound (A review). Acoust Phys. 49 (4), 369–388. https://doi.org/10.1134/1.1591291.

Chent, L., Haart, G., Hill, C.R., et al., 1993. Effect of blood perfusion on the ablation of liver parenchyma with high-intensity focused ultrasound. Phys. Med. Biol. 38 (11), 1661–1673. https://doi.org/10.1088/0031-9155/38/11/011.

Cheung, T.T., Chu, F.S., Jenkins, C.R., et al., 2012. Tolerance of high-intensity focused ultrasound ablation in patients with hepatocellular carcinoma. World J. Surg. 36 (10), 2420–2427. https://doi.org/10.1007/s00268-012-1660-7.

Curra, F.P., Mourad, P.D., Khokhlova, V.A., Cleveland, R.O., Crum, L.A., 2000. Numerical simulations of heating patterns and tissue temperature response due to high-intensity focused ultrasound. IEEE Trans. Ultrason. Ferroelectr. Freq. Control 47 (4), 1077–1089. https://doi.org/10.1109/58.852092.

Fenech, M., Garcia, D., Meiselman, H.J., Cloutier, G., 2009. A particle dynamic model of red blood cell aggregation kinetics. Ann. Biomed. Eng. 37 (11), 2299–2309. https://doi.org/10.1007/s10439-009-9775-1.

Gelat, P., Haar, G.T., Saffari, N., 2014. A comparison of methods for focusing the field of a HIFU array transducer through human ribs. Phys. Med. Biol. 59 (12), 3139–3171. https://doi.org/10.1088/0031-9155/59/12/3139.

Guntur, S.R., Choi, M.J., 2015. Influence of temperature-dependent thermal parameters on temperature elevation of tissue exposed to high-intensity focused ultrasound: numerical simulation. Ultrasound Med. Biol. 41 (3), 806–813. https://doi.org/10.1016/j.ultrasmedbio.2014.10.008.

Hamilton, M.F., Blackstock, D.T., 1998. Nonlinear Acoustics, first ed. Academic Press.

Hariharan, P., Myers, M.R., Banerjee, R.K., 2007. HIFU procedures at moderate intensities—effect of large blood vessels. Phys. Med. Biol. 52 (12), 3493–3513. https://doi.org/10.1088/0031-9155/52/12/011.

Hoskins, P., Martin, K., Thrush, A., 2010. Diagnostic Ultrasound Physics and Equipment, second ed. Cambridge University Press, New York.

Huang, C.W., Sun, M.K., Chen, B.T., Shieh, J., Chen, C.S., Chen, W.S., 2015. Simulation of thermal ablation by high-intensity focused ultrasound with temperature-dependent properties. Ultrason. Sonochem. 27, 456–465. https://doi.org/10.1016/j.ultsonch.2015.06.003.

Huang, J., 2002. Heating in Vascular Tissue and Flow-Through Tissue Phantoms Induced by Focused Ultrasound. PhD Dissertation. College of Engineering, Boston University.

Huang, J., Holt, R.G., Cleveland, R.O., Roy, R.A., 2004. Experimental validation of a tractable numerical model for focused ultrasound heating in flow-through tissue phantoms. J. Acoust. Soc. Am. 116 (4), 2451–2458. https://doi.org/10.1121/1.1787124.

Irastorza, R.M., Trujillo, M., Berjano, E., 2017. How coagulation zone size is underestimated in computer modeling of RF ablation by ignoring the cooling phase just after RF power is switched off. Int. J. Numer. Method. Biomed. Eng. 33 (11) https://doi.org/10.1002/cnm.2869.

Karimi, S., Dabagh, M., Vasava, P., Dadvar, M., Dabir, B., Jalali, P., 2014. Effect of rheological models on the hemodynamics within human aorta: CFD study on CT image-based geometry. J. Non-Newton. Fluid. 207, 42–52. https://doi.org/10.1016/j.jnnfm.2014.03.007.

Kolios, M.C., Sherar, M.D., Hunt, J.W., 1995. Large blood vessel cooling in heated tissues: a numerical study. Phys. Med. Biol. 40 (4), 477–494. https://doi.org/10.1088/0031-9155/40/4/001.

Kolios, M.C., Sherar, M.D., Hunt, J.W., 1996. Blood flow cooling and ultrasonic lesion formation. Med. Phys. 23 (7), 1287–1298. https://doi.org/10.1118/1.597694.

Li, J.J., Gu, M.F., Luo, G.Y., Liu, L.Z., Zhang, R., Xu, G.L., 2009. Complications of high intensity focused ultrasound for patients with hepatocellular carcinoma. Technol. Cancer Res. Treat. 8 (3), 217–224. https://doi.org/10.1177/153303460900800306.

Liu, Y., Liu, W.K., 2006. Rheology of red blood cell aggregation by computer simulation. J. Comput. Phys. 220 (1), 139–154. https://doi.org/10.1016/j.jcp.2006.05.010.

Mahoney, K., Fjield, T., McDannold, N., Clement, G., Hynynen, K., 2001. Comparison of modelled and observed in vivo temperature elevations induced by focused ultrasound: implications for treatment planning. Phys. Med. Biol. 46 (7), 1785–1798. https://doi.org/10.1088/0031-9155/46/7/304.

Meaney, P.M., Cahill, M.D., Haar, G.R.T., 1999. The intensity dependence of lesion position shift during focused ultrasound surgery. Ultrasound Med. Biol. 26 (3), 441–450. https://doi.org/10.1016/S0301-5629(99)00161-1.

Mehri, R., Mavriplis, C., Fenech, M., 2018. Red blood cell aggregates and their effect on non-Newtonian blood viscosity at low hematocrit in a two-fluid low shear rate microfluidic system. PLoS One 13 (7). https://doi.org/10.1371/journal.pone.0199911.

Peng, T., O'Neill, D.P., Payne, S.J., 2011. A two-equation coupled system for determination of liver tissue temperature during thermal ablation. Int. J. Heat Mass Transf. 54 (9-10), 2100–2109. https://doi.org/10.1016/j.ijheatmasstransfer.2010.12.019.

Pennes, H., 1948. Analysis of tissue and arterial blood temperatures in the resting human forearm. J. Appl. Physiol. 1 (2), 93–122. https://doi.org/10.1152/jappl.1948.1.2.93.

Rattanadecho, P.h., Keangin, P., 2013. Numerical study of heat transfer and blood flow in two-layered porous liver tissue during microwave ablation process using single and double slot antenna. Int. J. Heat Mass Transf. 58 (1-2), 457–470. https://doi.org/10.1016/j.ijheatmasstransfer.2012.10.043.

Ryerson, A.B., Eheman, C.R., Altekruse, S.F., et al., 2016. Annual report to the nation on the status of cancer,1975-2012, featuring the increasing incidence of liver cancer. Cancer 122 (9), 1312–1337. https://doi.org/10.1002/cncr.29936.

Samanipour, R., Maerefat, M., RezaeiNejad, H., 2013. Numerical study of the effect of ultrasound frequency on temperature distribution in layered tissue. J. Therm. Biol. 38 (6), 287–293. https://doi.org/10.1016/j.jtherbio.2013.03.002.

Sapareto, S.A., Dewey, W.C., 1984. Thermal dose determination in cancer therapy. Int. J. Radiat. Oncol. Biol. Phys. 10 (6), 787–800. https://doi.org/10.1016/0360-3016(84)90379-1.

Sheu, T.W.H., Solovchuk, M.A., Chen, A.W.J., Thiriet, M., 2011. On an acoustics–thermal–fluid coupling model for the prediction of temperature elevation in liver tumor. Int. J. Heat Mass Transf. 54 (17-18), 4117–4126. https://doi.org/10.1016/j.ijheatmasstransfer.2011.03.045.

Shih, T.C., Horng, T.L., Huang, H.W., et al., 2012. Numerical analysis of coupled effects of pulsatile blood flow and thermal relaxation time during thermal therapy. Int. J. Heat Mass Transf. 55 (13-14), 3763–3773. https://doi.org/10.1016/j.ijheatmasstransfer.2012.02.069.

Shung, K.K., 2006. Diagnostic Ultrasound: Imaging and Blood Flow Measurements, first ed. CRC Press.

Solovchuk, M.A., Sheu, T.W.H., Lin, W., Kuo, I., Thiriet, M., 2012. Simulation study on acoustic streaming and convective cooling in blood vessels during a high-intensity focused ultrasound thermal ablation. Int. J. Heat Mass Transf. 55 (4), 1261–1270. https://doi.org/10.1016/j.ijheatmasstransfer.2011.09.023.

Solovchuk, M.A., Sheu, T.W.H., Thiriet, M., Lin, W.L., 2013. On a computational study for investigating acoustic streaming and heating during focused ultrasound ablation of liver tumor. Appl. Therm. Eng. 56 (1-2), 62–76. https://doi.org/10.1016/j.applthermaleng.2013.02.041.

Solovchuk, M., Sheu, T.W.H., Thiriet, M., 2013. Simulation of nonlinear Westervelt equation for the investigation of acoustic streaming and nonlinear propagation effects. J. Acoust. Soc. Am. 134 (5), 3931–3942. https://doi.org/10.1121/1.4821201.

Solovchuk, M., Sheu, T., Thiriet, M., 2014. Image-based computational model for focused ultrasound ablation of liver tumor. J. Comput. Surg. 1 (4) https://doi.org/10.1186/2194-3990-1-4.

Tungjitkusolmun, S., Staelin, S.T., Haemmerich, D., et al., 2002. Three-dimensional finite-element analyses for radio-frequency hepatic tumor ablation. IEEE T. Bio-med. Eng. 49 (1), 3–9. https://doi.org/10.1109/10.972834.

Zhou, Y., Kargl, S.G., Hwang, J.H., 2011. The effect of the scanning pathway in high-intensity focused ultrasound therapy on lesion production. Ultrasound Med. Biol. 37 (9), 1457–1468. https://doi.org/10.1016/j.ultrasmedbio.2011.05.848.

Zhou, Y., 2013. Generation of uniform lesions in high intensity focused ultrasound ablation. Ultrasonics 53 (2), 495–505. https://doi.org/10.1016/j.ultras.2012.09.001.